JACS
JOURNAL OF THE AMERICAN CHEMICAL SOCIETY
pubs.acs.org/JACS
Article

Stereodivergent Construction of *trans*-Decalin-Based Terpenoids

Samantha L. Barlock, Alexander S. Shved, Kayla D. Landers, Binh Khanh Mai, Shogo Fujiki, Peter C. Ryffel, Wai Yam Lo, Andrew G. Feng, Nicholas W. Wade, Lingyang Zhu, Viet D. Nguyen, David A. Petrone,* Scott E. Denmark,* and David Sarlah*

Cite This: https://doi.org/10.1021/jacs.6c01881

Read Online

ACCESS | Metrics & More | Article Recommendations | Supporting Information

ABSTRACT: Thousands of highly oxygenated terpenoid natural products contain a common *trans*-decalin core bearing oxidized substituents in either the equatorial or axial configuration at the C(4) quaternary center. We report an expedient route to a versatile terpenoid building block primed for elaboration into numerous complex natural products. This intermediate is provided from (*R*)-carvone, a cheap and abundant chiral pool material, in three steps through a diastereodivergent, intramolecular carboborylation reaction. Notably, this method uniquely provides either equatorial or axial functionalized products from a single, common precursor. Identification of optimal ligands required extensive screening efforts, facilitated in part by high-throughput experimentation (HTE) and the construction of an algorithmically guided, combinatorial, in silico library, which identified the highest performing axial-selective ligand. The key interactions responsible for the observed high diastereoselectivity were elucidated with computational analysis, and the synthetic utility of this method was demonstrated in the total synthesis of several diterpenoid natural products.

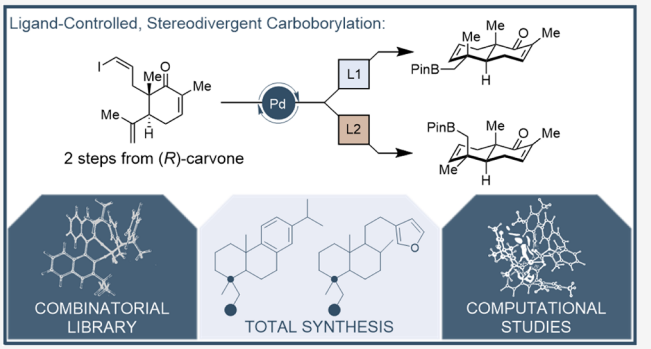

INTRODUCTION

With more than 80,000 known members, terpenoids represent the largest family of natural products.[1] This vast chemical library, termed the terpenome, contains natural products with broad structural diversity.[2] Terpenoids are most common in plants, in which it has been estimated that thousands of distinct family members play critical roles in biological processes including growth and defense.[3] The chemical diversity of these metabolites translates to a range of important biological activities, and thus the terpenome serves as an abundant source of potential pharmaceutical candidates.[4,5]

Despite their promise in drug discovery, the structural complexity of terpenoids is often a barrier to their preparation and use in medicinal chemistry campaigns.[6] Though the total synthesis of terpenes is a well-established field, the pursuit of complex targets has relied on the use of highly tailored strategies that limit access to structural analogs, especially stereoisomers.[7,8] Importantly, stereoisomers can demonstrate distinct pharmacological activities,[9] as exemplified by the C(4)-epimeric natural products *trans*- and *cis*-communic acid (Figure 1A).[10,11] The development of practical, stereodivergent strategies to construct versatile building blocks would offer great utility in the synthesis of diverse bioactive terpenoids.

BACKGROUND

The *trans*-decalin ring system is found in thousands of natural products and represents a valuable terpenoid building block (Figure 1A).[12−17] Many terpenoids are distinguished by unique oxidation patterns decorating a common carbon skeleton, and a persistent challenge in terpenoid synthesis is stereoselective installation of functionalized substituents at the C(4) carbon center (i.e., axial vs equatorial functionalization). The lack of general and efficient methods to achieve this goal limits the synthetic accessibility of the nearly 15,000 natural products characterized to date that bear oxidized substituents at C(4).[18]

The Wieland−Miescher ketone (WMK) has long served as a cornerstone of complex terpenoid synthesis as it provides facile access to *trans*-decalin structures.[19,20] Derivatization of the WMK can be leveraged to procure valuable stereoisomers through selective installation of oxidized substituents in either the axial or equatorial position at C(4) (Figure 1B).[21−25] However, this early divergence point necessitates tedious

Received: January 26, 2026
Revised: March 3, 2026
Accepted: March 10, 2026

https://doi.org/10.1021/jacs.6c01881
J. Am. Chem. Soc. XXXX, XXX, XXX−XXX

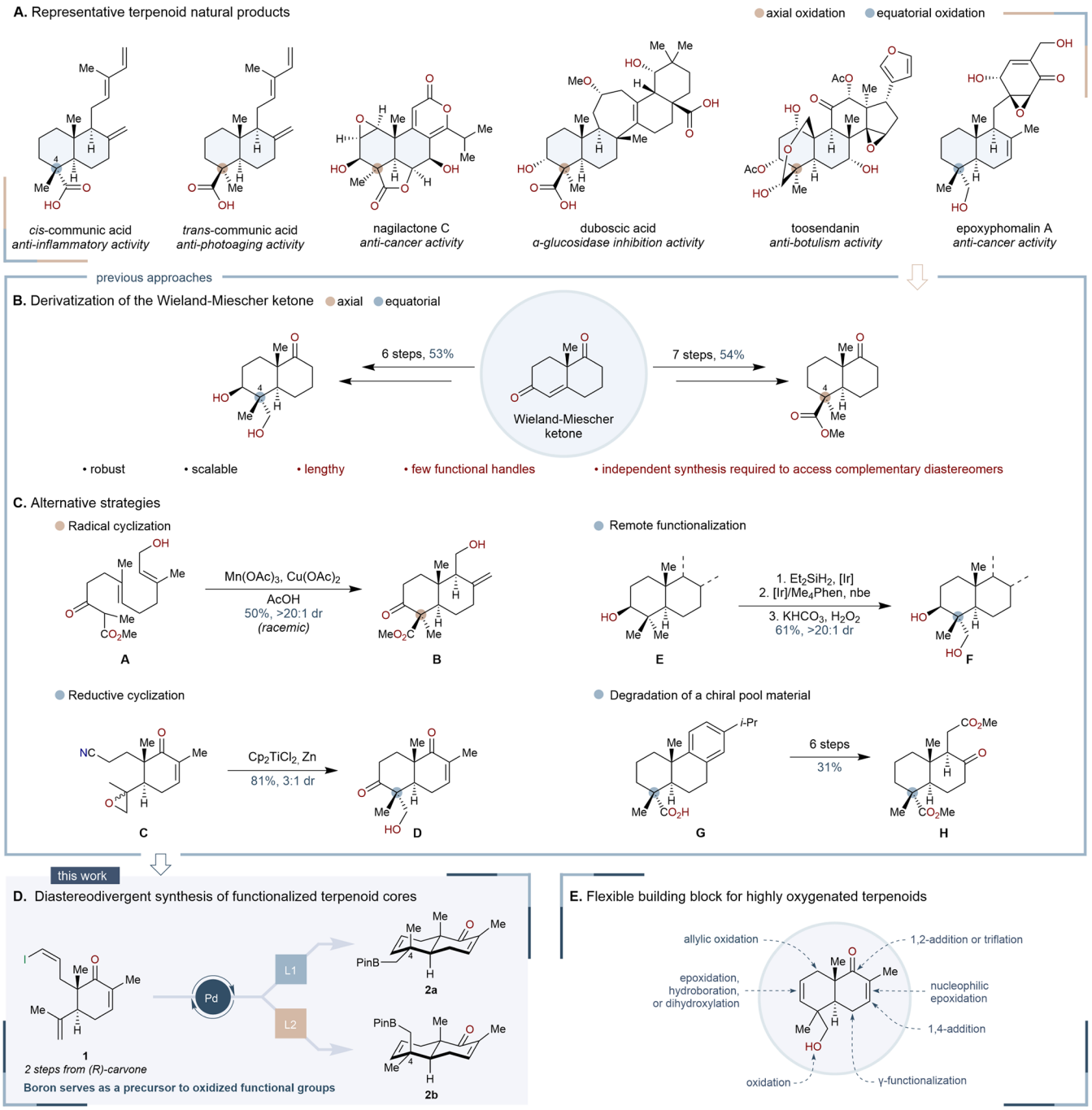

Figure 1. (A) Structures of representative bioactive terpenoids bearing oxidized substituents at C(4), (B) accessing oxidized substituents at C(4) via derivatization of the Wieland−Miescher ketone, (C) alternative strategies to construct functionalized *trans*-decalin intermediates, (D) this work: construction of versatile terpenoid building blocks via a diastereodivergent carboborylation/oxidation reaction, and (E) potential transformations facilitating downstream elaboration into highly oxygenated terpenoids.

independent synthesis (>6 steps) to obtain the individual C(4) epimers.

Although alternative strategies to construct functionalized *trans*-decalins have been developed, these methods preferentially yield a single stereoisomer as dictated by substrate control. Processes such as cationic polyene,[26] radical[27] (Figure 1C, **A** → **B**) or reductive cyclizations[28,29] (Figure 1C, **C** → **D**) demonstrate greater efficiency than derivatization of the WMK but do not provide a means to access complementary C(4) epimers in high selectivity. Established chiral pool approaches can similarly be leveraged to rapidly build *trans*-decalin structures but require further manipulations to achieve the desired C(4) functionalization.[30,31] Collectively, these methods favor installation of oxidized substituents in the equatorial position. Furthermore, recent advances in remote functionalization[32−34] deliver exclusive oxidation of the equatorial substituent. To date, only the WMK provides a general platform to install oxidized substituents in the axial position of the C(4) quaternary center.

Significant barriers to installing oxidized C(4) substituents persist despite modern efforts to improve efficiency and stereoselectivity.[29,30,34] Consequently, procedures have been

https://doi.org/10.1021/jacs.6c01881
J. Am. Chem. Soc. XXXX, XXX, XXX−XXX

developed to provide functionalized decalin intermediates through degradation of chiral pool materials in recent works (Figure 1C, **G** → **H**) rather than pursue de novo decalin core construction.[35] The development of a method that provides both the stereochemical flexibility offered by derivatization of the WMK and the high efficiency of alternative cyclization-based approaches would streamline the synthesis of decalin-containing terpenoids. Although achieving stereodivergence is a challenging undertaking in its own right, it also requires overcoming the longstanding dearth of methods that can facilitate axial-selective functionalization.

Herein, we report a stereodivergent, palladium-catalyzed borylative cyclization reaction which enables construction of *trans*-decalin intermediates bearing either equatorial or axial functionalized C(4) substituents from a common precursor (Figure 1D). This efficient method selectively provides diastereomeric building blocks primed for elaboration into highly oxygenated terpenoid natural products from (*R*)-carvone (Figure 1E). Identification of optimal ligands required extensive screening efforts facilitated in part by high-throughput experimentation (HTE) and construction of an algorithmically guided, combinatorial, in silico library of potential ligands. The key interactions responsible for the observed high diastereoselectivity were elucidated with computational analysis. Finally, the synthetic utility of this strategy was demonstrated in the total synthesis of seven abietane diterpenoids, including high-value C(19) oxidized family members with low natural abundances, and several labdane diterpenoids bearing axially disposed C(4) functionalization.

RESULTS AND DISCUSSION

Reaction Development

Inspired by previous chiral pool approaches (see Supporting Information for details),[29−31] we proposed a diastereodivergent, intramolecular, domino Heck/borylation/oxidation strategy to directly afford functionalized terpenoid building blocks from known vinyl iodide 1 (Figure 2).[31] Fortunately, trapping neopentyl-Pd(II) intermediates is a well-documented transformation with a range of nucleophiles.[36−43] We expected that installation of a boron-based functional handle would provide expedient access to oxygenated derivatives, and we were encouraged in this pursuit by several reports of domino Heck/borylation reactions.[44−48] Though we recently explored a carboborylation strategy to prepare the *trans*-decalin core of nimbolide,[49] the observed stereoselectivity was a consequence of substrate bias exerted by a tailored cyclization precursor. We envisioned that the development of a catalyst-controlled stereodivergent carboborylation reaction would provide a powerful platform to prepare functionalized *trans*-decalin building blocks suitable for more diverse applications in terpenoid synthesis.

To access the feasibility of constructing the target decalin framework with an intramolecular carboborylation reaction, we applied cationic arylborylation conditions with (*R*)-BINAP previously disclosed by Lu and coworkers[47] which delivered the desired cyclization products **2a** and **2b**, albeit in poor yield (Figure 2, **L1**). Encouraged by this preliminary result, the performances of 32 ligands were evaluated under cationic conditions (Figure 2, see Supporting Information, Table S1, for full details). Moderate to high yields were achieved with PHOX and Phosferrox ligands, with **L12** delivering **2a** in 97% yield and >20:1 dr favoring equatorial borylation. Fortunately, commercially available **L11** provided 87% yield while maintaining >20:1 dr (eq/ax). Josiphos, Taniaphos, and JoSPOphos ligands (**L6**−**L8**) performed poorly by comparison. Further experiments revealed that other bases, silver additives, and solvents resulted in diminished yields and/or diastereoselectivities (see Supporting Information, Table S2, for details).

Extensive surveying revealed that cationic reaction conditions strongly favored equatorial carbopalladation, thus leading to rapid identification of a catalytic system that delivered equatorial borylation product **2a** in excellent yield and diastereoselectivity. Conversely, this intrinsic bias in reactivity hindered identification of a ligand that enabled selective formation of axial borylation product **2b**. It is well-precedented that cationic and neutral Heck reaction manifolds can provide divergent stereochemical outcomes,[50] and we hypothesized that conditions favoring a neutral Heck pathway may afford axial selectivity. To obtain a reactivity baseline for neutral conditions, a catalyst system excluding a silver additive and comprised of tris(dibenzylideneacetone)dipalladium(0) [$Pd_2(dba)_3$], KOAc, and B_2Pin_2 in DMF was evaluated. Therein, borylated product **2** was obtained in 70% yield as a 1:1 mixture of equatorial and axial diastereomers alongside complex mixtures of cyclopropanation byproducts (see Supporting Information, Table S3, for details).

We then examined the effects of ligands under neutral reaction conditions. Although $Pd_2(dba)_3$ is a widely used precursor to soluble Pd complexes,[51] it is known to exhibit facile decomposition to Pd nanoparticles[52] and variable rates of phosphine metalation dependent on ligand structure.[53] In anticipation of extensive small-scale ligand screening, we employed ^{DMP}DAB-Pd-MAH (Figure 2), a reliable and convenient Pd(0) source bearing *N*,*N*′-diaryldiazabutadiene and maleic anhydride ligands that facilitates in situ catalyst preparation.[54] First, a diverse library of approximately 70 chiral bisphosphines was evaluated in microscale HTE format (see Supporting Information, Table S4). This ligand class generally suffered from low yields, with fewer than 20 bisphosphines delivering detectable quantities of the desired products. We then explored a variety of ligand classes (Figure 2, see Supporting Information, Table S5, for full details) and identified N-heterocyclic carbene (NHC) ligand **L18** which provided good yield and a slight preference for axial product **2b**. In subsequent studies, a library of 24 chiral NHC ligands failed to improve selectivity (see Supporting Information, Table S6). Fortunately, this survey also identified phosphoramidites as a promising ligand class. Although the performance of (*R*)-monophos (**L19**) was unexceptional, further exploration of phosphoramidite ligands was appealing on account of their modularity, ease of synthesis, and wide structural, electronic, and steric tunability.

Identification of an optimal ligand structure is a challenging task commonly resolved with extensive surveying of catalyst libraries.[55,56] This approach is reliant on commercial availability of appropriate catalysts. Instead, we opted to leverage diversity analysis of a large molecular in silico library,[57−60] as previously demonstrated in the context of binaphthyl-derived phosphoric acid,[61,62] disulfonimide,[63] and copper·bis(oxazoline) catalysts.[64] In these studies, unsupervised diversity analysis alone was sufficient to discover high performing catalyst and ligand subclasses, regardless of the success of downstream extrapolative regression modeling.

https://doi.org/10.1021/jacs.6c01881
J. Am. Chem. Soc. XXXX, XXX, XXX−XXX

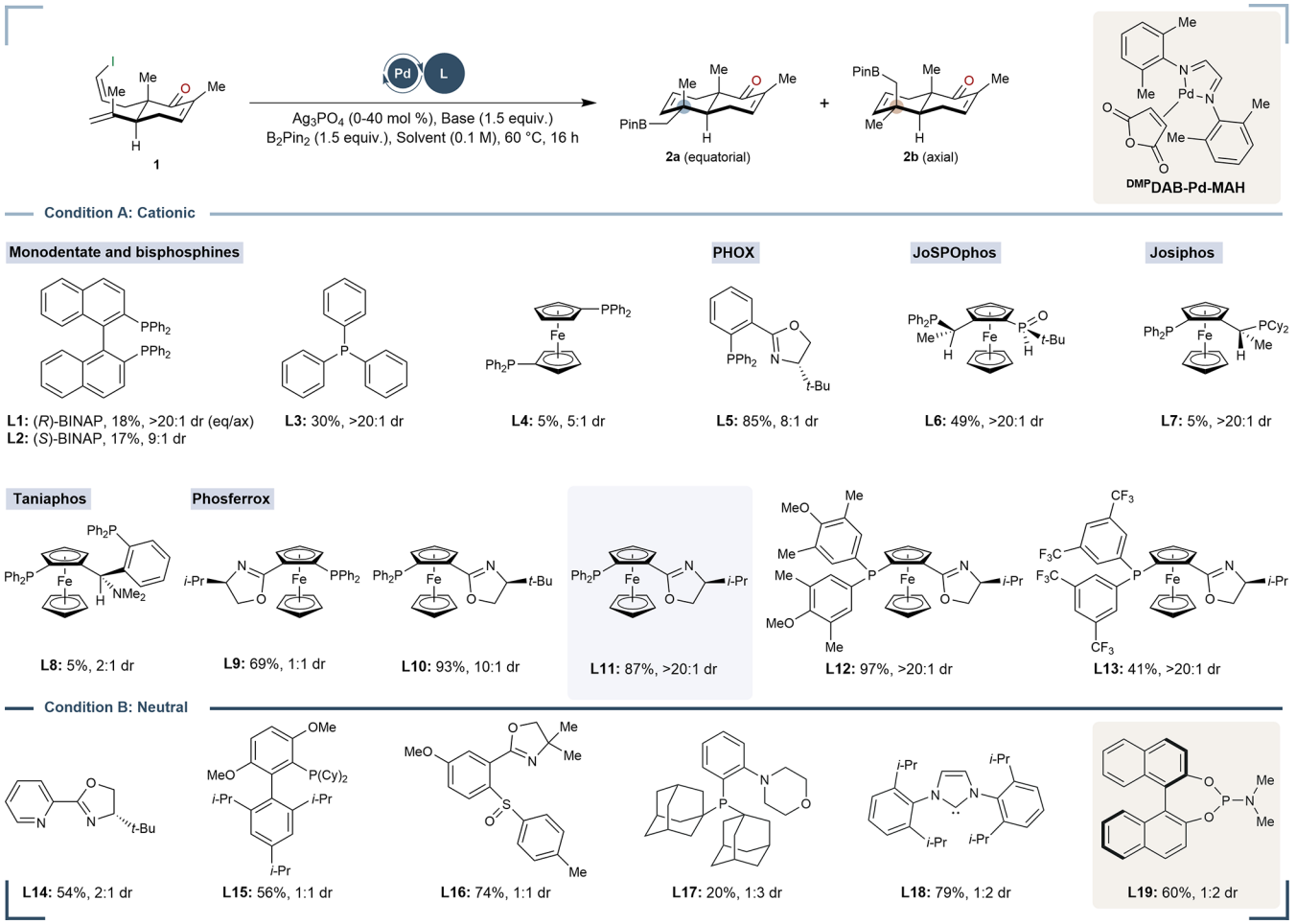

Figure 2. Evaluation of ligand performance under cationic and neutral conditions. Yields were determined by SFC or ^{1}H NMR analysis relative to 1,3,5,-trimethoxybenzene internal standard. **Condition A:** $[(\eta^3\text{-allyl})PdCl]_2$ (4 mol %), ligand (9 mol %), Ag_3PO_4 (40 mol %), K_2CO_3 (1.5 equiv), B_2Pin_2 (1.5 equiv), MeCN (0.1 M), 60 °C, 16 h. **Condition B:** ^{DMP}DAB-Pd-MAH (10 mol %), ligand (20 mol %), KOAc (1.5 equiv), B_2Pin_2 (1.5 equiv), DMF (0.1 M), 60 °C, 16 h.

Therefore, we anticipated diversity analysis would identify regions of chemical space containing active substructures and set out to generate a highly diverse set of phosphoramidite ligands (referred to as a Universal Training Set, UTS).

A large in silico library of phosphoramidite structures was created by combining BINOL cores bearing unique 3,3′-substituents and amine fragments (see Supporting Information, Tables S15−S17) using in-house developed software, molli (Figure 3A).[65] We anticipated that exploring a *full combinatorial* phosphoramidite library, constructed from the 1,478 BINOL structures previously disclosed by the Denmark group[63] and 681 distinct amines, would be computationally infeasible. Accordingly, we focused our attention on the intersection of a reduced, yet still highly diverse BINOL subset with all amines (see Supporting Information for details). The resulting phosphoramidite structures were featurized for steric (ASO)[61] and electronic (AEIF)[62,66] spatial localization in a conformationally dependent manner (CREST[67]/GFN2-xTB[68]//RDKit[69,70]). A subset of 17,676 structures (indicated by teal dots, Figure 3B) was used to inform the cluster centroid locations [white X's], and expert curation of centroid neighbors identified 20 UTS structures. A total of 49 phosphoramidites were evaluated experimentally (indicated by pink dots, with top performing ligands highlighted by a yellow hexagon), including 11 UTS structures, 16 control ligands containing an unsubstituted BINOL backbone, and 22 ligands designed to test perturbations of R^1 substitution or amine structure (see Supporting Information, Table S8, for ligand structures). An expanded library of 56,943 items [dark blue dots] was later constructed to encompass all permutations of substituents used in this work, including validation structures. We note that the selected ligand set (UTS + validation structures) extends significantly beyond the boundaries of commercially available structures [purple squares].

Evaluation of the aforementioned ligand set was carried out using 10 mol % $Pd(OAc)_2$, 20 mol % ligand, B_2Pin_2 (1.5 equiv), potassium 2-ethylhexanoate[71] (2-KEH, 1.5 equiv), 1,4-dioxane (0.1 M), 60 °C (see Supporting Information, Table S7, for optimization details). These studies identified **L20,** which delivered **2b** in 62% yield and >20:1 dr favoring axial borylation (Figure 3C, entry 1). The comparative performance of structurally similar ligands revealed that reactivity was highly sensitive to the structures of both the BINOL and amine components. For example, simple replacement of the trifluoromethyl groups with methyl groups resulted in significant deterioration of selectivity (entry 2). It is noteworthy that the 3,5-bis(trifluoromethyl)phenyl substitution was conserved across all but one of the six ligands that promoted a high level of axial selectivity (>10:1 dr, ax/eq) (see

https://doi.org/10.1021/jacs.6c01881
J. Am. Chem. Soc. XXXX, XXX, XXX−XXX

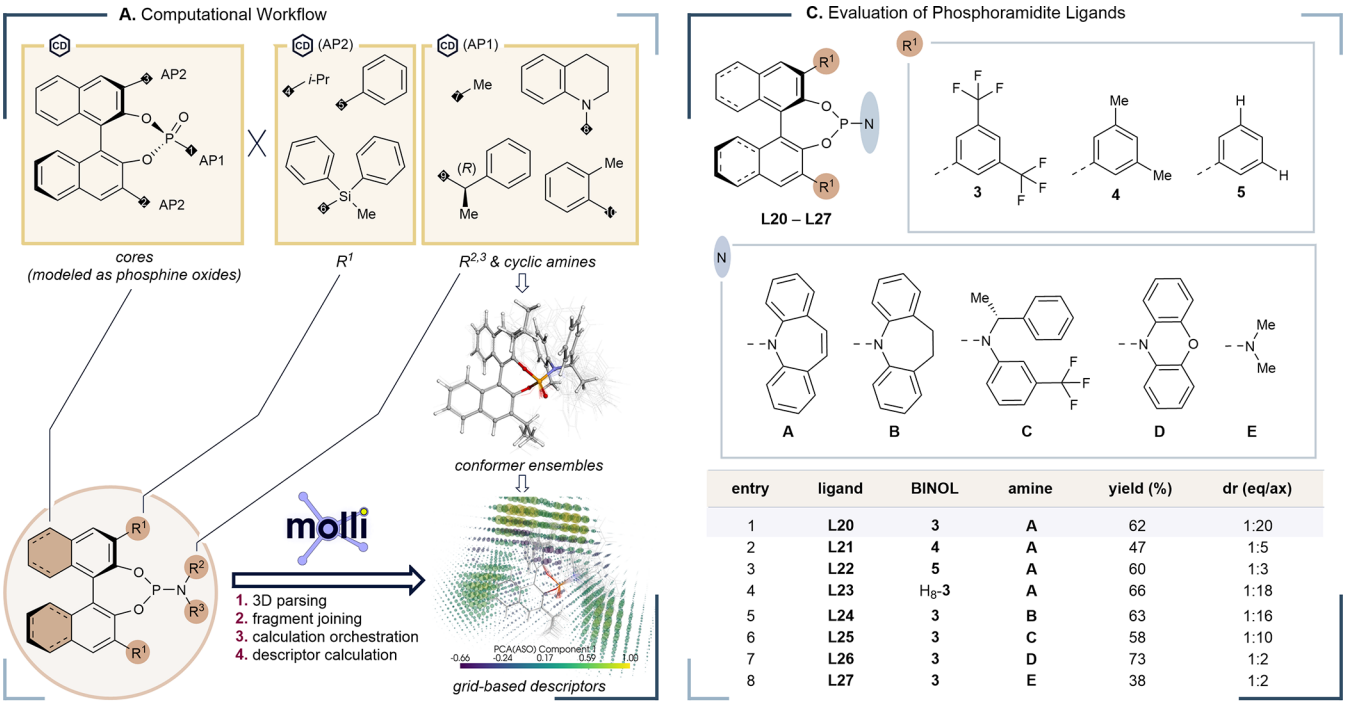

entry	ligand	BINOL	amine	yield (%)	dr (eq/ax)
1	L20	3	A	62	1:20
2	L21	4	A	47	1:5
3	L22	5	A	60	1:3
4	L23	H_8-3	A	66	1:18
5	L24	3	B	63	1:16
6	L25	3	C	58	1:10
7	L26	3	D	73	1:2
8	L27	3	E	38	1:2

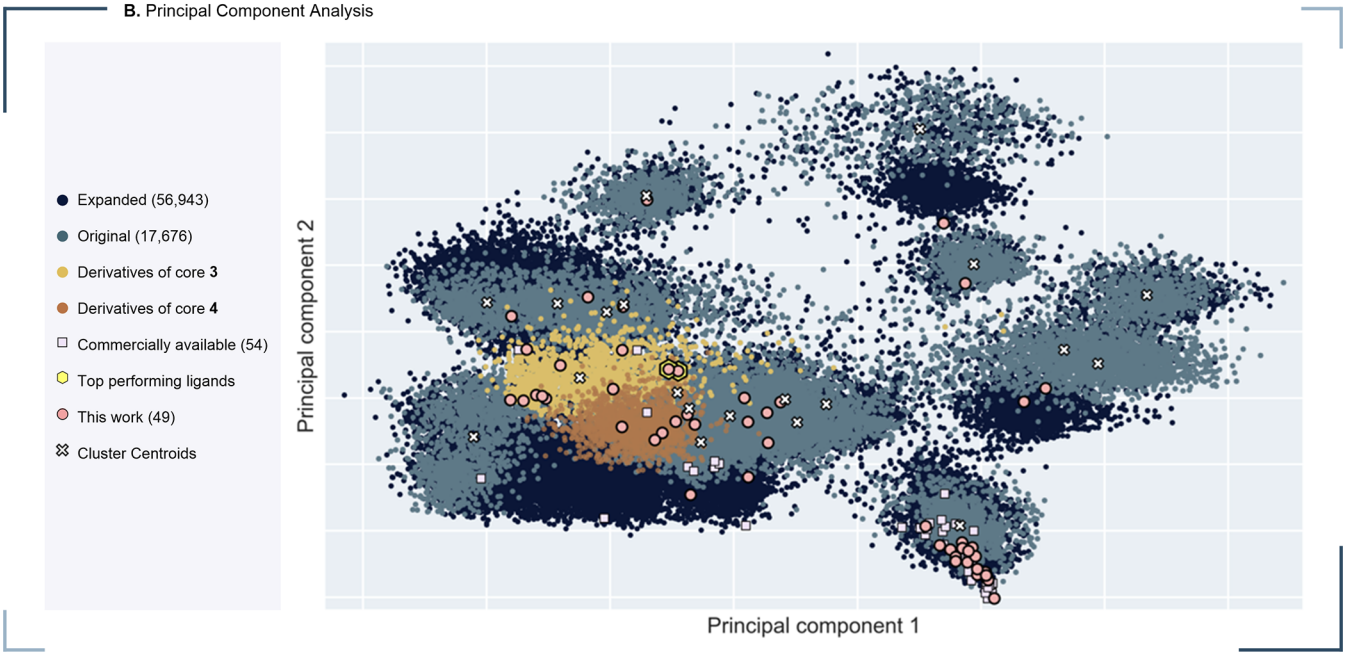

Figure 3. (A) Computational workflow for combinatorial library assembly, conformer generation and refinement orchestration, and 3D descriptor calculation using molli software. (B) Principal Component projection of the ASO + AEIF chemical space, highlighting the distribution of key structures. (C) Notable results from the HTE screening featuring the highest performing ligands and key control structures. **Conditions:** $Pd(OAc)_2$ (10 mol %), ligand (20 mol %), potassium 2-ethylhexanoate (1.5 equiv), B_2Pin_2 (1.5 equiv), 1,4-dioxane (0.1 M), 60 °C, 16 h.

Supporting Information, Table S9, for phosphoramidite survey results). Similarly, replacement of the dibenzazepine motif (**A**) with phenoxazine (**D**) resulted in significantly diminished selectivity, even when the 3,5-bis(trifluoromethyl)phenyl substituted BINOL was conserved (entry 7). Selectivity was not markedly influenced by minor structural alterations to the ligand, including use of the H_8−BINOL backbone (entry 4) or employment of the saturated dibenzazepine central ring (entry 5).

Applications in Total Synthesis

We developed a multigram-scale carboborylation/oxidation protocol to apply the diastereodivergent carboborylation strategy in total synthesis (Figure 4A). Equatorial-selective carboborylation, mediated by Phosferrox ligand **L11**, and subsequent oxidation with sodium perborate delivered a 10:1 mixture of enones **6a** and **6b** in 63% combined yield on four-gram scale. Recrystallization then provided **6a** as a single diastereomer (>20:1 dr, eq/ax) in 54% yield. Alternatively, an axial-selective protocol mediated by phosphoramidite ligand

https://doi.org/10.1021/jacs.6c01881
J. Am. Chem. Soc. XXXX, XXX, XXX−XXX

L20 yielded **6b** as a single diastereomer (1:>20 dr, eq/ax) favoring axial functionalization in 67% yield on four-gram scale. Compared to the traditionally employed Wieland−Miescher ketone, enones **6a** and **6b** provide a more advanced entry point to the synthesis of oxygenated terpenoids. With efficient access to versatile building blocks, we were positioned to pursue divergent total syntheses of several terpenoid natural products.

Abietanes

Approximately 300 known dehydroabietanes are distinguished by unique oxidation patterns (Figure 4B).[72] While abietanes bearing C(18) oxidation (e.g., dehydroabietic acid) are common chiral pool materials, those possessing C(19) oxidation have significantly lower natural abundances and limited commercial availability.[73,74] Reports describing the semisynthesis of C(19) oxidized abietanes frequently require prohibitively expensive starting materials that are obtained through extraction from pine resins or arduous inversion of the C(4) quaternary center of dehydroabietic acid (>9 steps).[75−77] The stereodivergent carboborylation reaction was shown to be a powerful tool to access structurally diverse abietanes, as demonstrated in the synthesis of seven natural products (**11**−**17**) from enones **6a** and **6b**.

A uniform synthetic sequence was applied to each diastereomeric building block to construct the abietane skeleton (Figure 4C, top). Following silyl protection of the C(4) hydroxymethyl group of **6**, one-pot conjugate reduction and subsequent enolate trapping with Comins' reagent furnished coupling partner **7**. Sequential Heck coupling with ethyl acrylate, 6π electrocyclization of an in situ generated trienyl ketene acetal, and ester hydrolysis then delivered tricyclic product **9**.[78] Lastly, triflation and Negishi coupling with *i*-PrMgCl yielded the complete abietane skeleton **10**.[79]

After establishing the abietane core, we pursued the synthesis of seven distinct natural products (Figure 4C, bottom). Reduction of the A-ring alkene and TBS deprotection afforded dehydroabietol (**11**) or 4-*epi*-dehydroabietol (**12**).[80] Dehydroabietic acid (**13**) and callitrisic acid (**14**) were obtained, respectively, from direct oxidation of **11** and **12** to the corresponding carboxylic acids.[81] In the equatorial series, reduction of the A-ring alkene followed by benzylic oxidation with CrO_3 and silyl ether deprotection furnished 7-oxo-abietol (**15**),[82] whereas sequential treatment of phthaloyl peroxide[83] (PPO) followed by HF delivered 18-hydroxyferruginol (**16**).[84] Lastly, in the axial series, application of a hydroboration/oxidation protocol to **10** followed by silyl ether deprotection delivered 8,11,13-abietatriene-2,19-diol (**17**).[85]

Hypophyllins E and F

Recently, a series of unique labdane natural products was isolated from the ornamental plant *Hypoestes phyllostachya* "Rosea" (Figure 4D). Zhao and coworkers characterized rearranged labdane-type diterpenoids hypophyllins A−F (**18**−**23**), of which several family members demonstrate potent vasorelaxant activity.[86] Hypophyllin D (**21**), the most structurally complex family member, features an uncommon 8,9-dioxatricyclic[4.2.1.$1^{3,7}$]decane moiety. Notably, each of these natural products bears axial substituent oxidation at C(4). Considering the scarcity of methods delivering axial functionalization, the stereodivergent carboborylation strategy is well-positioned to enable pursuit of complex labdanes such as hypophyllin D (**21**). Toward this end, we targeted hypophyllin E (**22**), the proposed biosynthetic precursor to hypophyllins A−D (**18**−**21**), to establish an entry point to this family of natural products.

Our efforts began with selective hydrogenation of the electron-rich double bond in enone **6b** using Wilkinson's catalyst (Figure 4E).[87] Sequential oxidation of the axially disposed hydroxymethyl group to the corresponding carboxylic acid, methyl esterification, and triflation of the B-ring enone then provided dienol triflate **24.** Notably, use of 2-azaadamantane-*N*-oxyl (AZADOL) was necessary to achieve direct oxidation of the primary alcohol to a carboxylic acid.[88] Following selective dihydroxylation of the more accessible double bond of dienol triflate **24**, the full hypophyllin carbon skeleton was established by Kuwajima-Urabe coupling with silyl enol ether **25**.[89,90] Following liberation of the acyl furan motif with TBAF, Crabtree's catalyst affected hydroxyl-directed hydrogenation of the tetrasubstituted double bond to deliver diol **26**. Optimization studies indicated that substitution of the PF_6^- counterion with $BArF^-$ and the use of elevated H_2 pressure provided superior hydrogenation yields.[91] Finally, inversion of the C(5) alcohol was achieved by sequential treatment of **26** with IBX and sodium triacetoxyborohydride to deliver hypophyllin E (**22**).[92] The penultimate IBX oxidation yielded a mixture of products, including hypophyllin F (**23**) (see Supporting Information for details).

Investigation of Diastereoselectivity

To gain detailed insights into the origin of diastereoselectivity, density functional theory (DFT) calculations were carried out at the M06/6-311+G(d,p)-SDD(Pd, Fe, Ag, I)/SMD//B3LYP-D3/6-31G(d)-SDD(Pd, Fe, Ag, I) level of theory for axial-selective reaction conditions with phosphoramidite ligand **L20** (Figure 5, see Supporting Information for details). Initially, ligand exchange with Pd(0) species **I-1** affords Pd(0)-substrate complex **I-2**. The activation barrier for the subsequent oxidative addition through transition state **TS-1** is calculated to be 19.0 kcal/mol relative to **I-1**. From the resulting vinylPd(II) intermediate **I-3**, an ethyl hexanoate anion (modeled by isobutyrate anion to reduce computational cost) coordinates to the Pd center to afford a more stable Pd(II) "ate" complex **I-4**.[71] Then, dissociation of the iodide ion and coordination of the alkene moiety generates the reactive Pd(II)−alkene π-complexes **I-5-ax** (black) and **I-5-eq** (blue). Migratory insertion can occur at either the (*Si*)- or (*Re*)-faces of the alkene to form a new C−C single bond via **TS-2-ax** and **TS-2-eq** with activation barriers of 22.7 and 24.9 kcal/mol relative to **I-4**, respectively. The resulting Pd(II)-alkyl intermediates **I-6-ax**/**I-6-eq** undergo transmetalation in a stepwise fashion: barrierless complexation of B_2Pin_2 to the isobutyrate anion followed by B−B bond cleavage generates Pd(II)-boryl species **I-7-ax**/**I-7-eq**. The activation barriers for the transmetalation transition states **TS-3-ax** and **TS-3-eq** are calculated to be 20.6 and 21.9 kcal/mol relative to **I-6-ax** and **I-6-eq**, respectively. Finally, **I-7-ax**/**I-7-eq** undergo rapid reductive elimination via **TS-4-ax**/**TS-4-eq** to provide axial and equatorial products **2b** and **2a**, respectively. According to this energy profile, migratory insertion (via **TS-2**) is both the turnover-limiting and diastereoselectivity-determining step with a Gibbs free energy difference of 2.2 kcal/mol corresponding to 39:1 dr favoring the axial diastereomer. The calculated selectivity is in good agreement with the experimental result of 20:1 dr (ax/eq).

Thorough analyses of the migratory insertion transition states **TS-2-ax** and **TS-2-eq** were performed (Figure 6).

https://doi.org/10.1021/jacs.6c01881
J. Am. Chem. Soc. XXXX, XXX, XXX−XXX

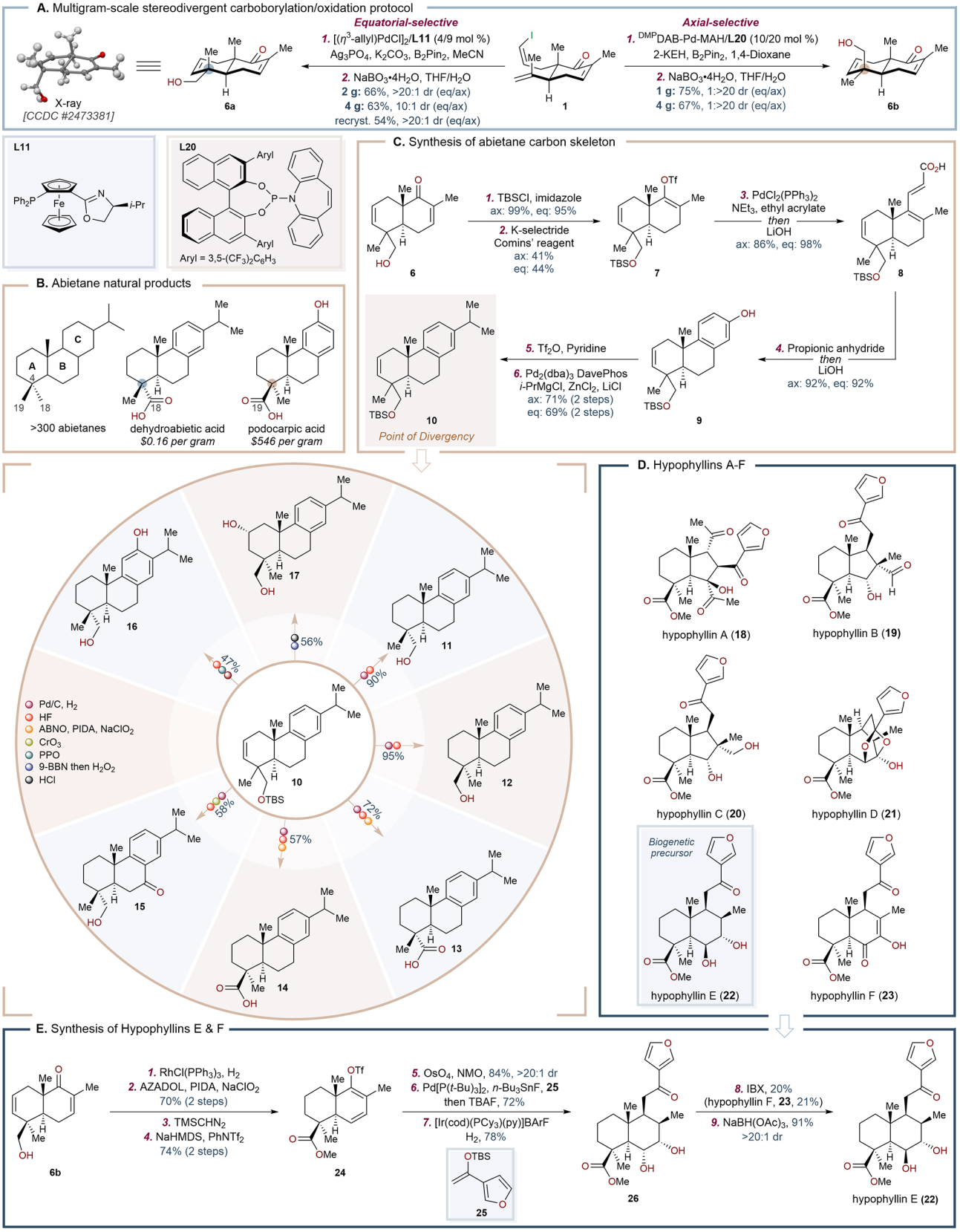

Figure 4. Applications in total synthesis. (A) Multigram scale diastereodivergent carboborylation/oxidation protocol, (B) representative abietane natural products, (C) synthesis of structurally diverse dehydroabietanes, (D) labdane natural products isolated from *Hypoestes phyllostachya*"Rosea" and (E) synthesis of hypophyllins E and F.

Noncovalent interaction (NCI) analysis[93] indicates that **TS-2-ax** is stabilized by strong dispersion/electrostatic interactions between substrate **1** and the CF_3 groups of phosphoramidite ligand **L20** (indicated by green to blue regions, Figure

https://doi.org/10.1021/jacs.6c01881
J. Am. Chem. Soc. XXXX, XXX, XXX−XXX

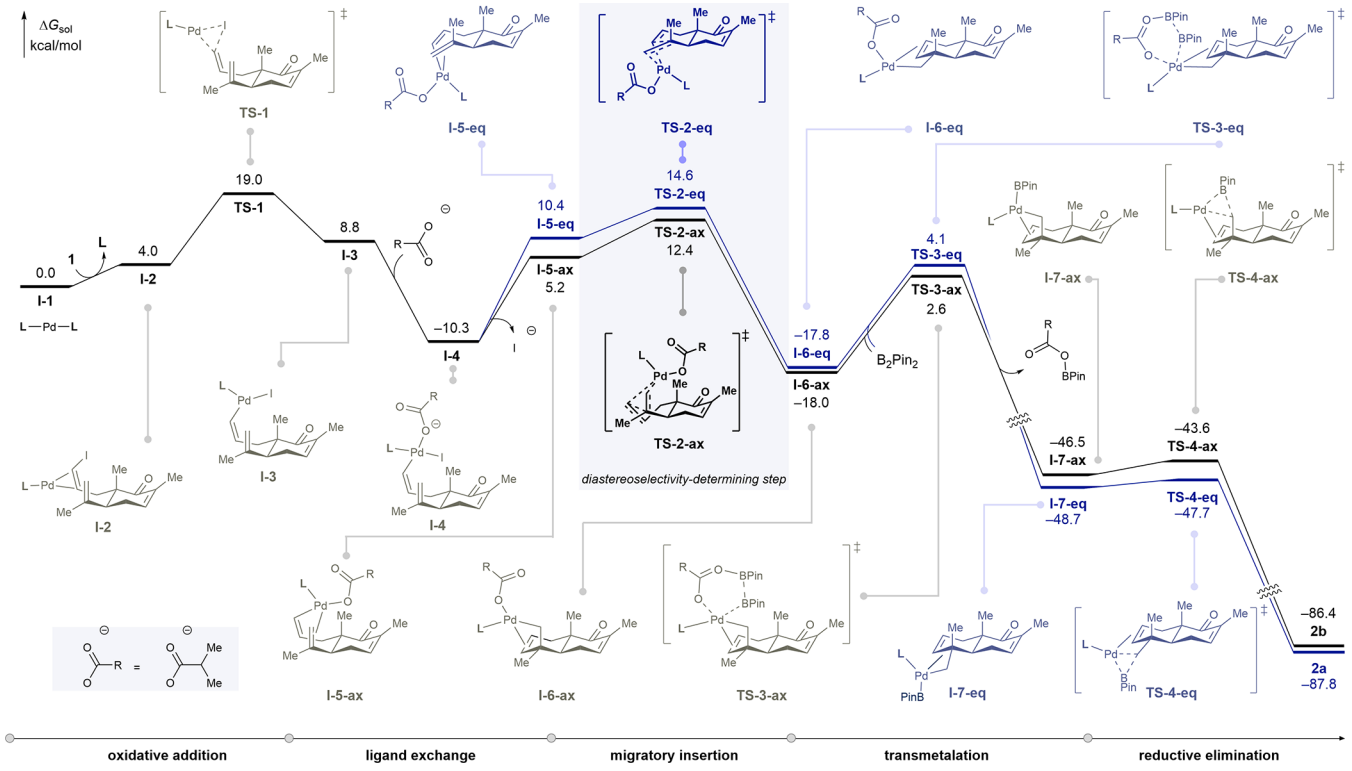

Figure 5. Computed free energy profile (in kcal/mol) for the Pd-catalyzed carboborylation reaction under axial-selective conditions using phosphoramidite ligand **L20**. The ethyl hexanoate anion is replaced by isobutyrate anion to reduce computational cost.

6A).[94−96] Distortion-interaction analysis (DIA)[97,98] was then performed to dissect the activation energy into energy terms (Figure 6B). Minor contributing energy terms describing the isobutyrate ion were not analyzed. DIA calculations reveal that substrate−ligand NCIs play a crucial role in diastereoselectivity with an energy difference $\Delta\Delta E_{\text{int-space}}$ of −4.5 kcal/mol favoring the axial product (Figure 6B). To quantitatively deconstruct NCIs into chemically meaningful energy terms, energy decomposition analysis (EDA) was performed using the Symmetry-Adapted Perturbation Theory algorithm.[99−102] EDA calculations show that in **TS-2-ax**, electrostatic and dispersion interactions are 1.7 and 3.8 kcal/mol stronger (i.e., more negative) than those in **TS-2-eq**, which is consistent with the NCI regions shown in Figure 6A.

To further study the effects of the CF_3 groups on diastereoselectivity, calculations were performed to describe migratory insertion transition states using 3,5-bis(methyl)-phenyl-substituted ligand **L21**. The Gibbs free energy difference between **TS-2′-ax** and **TS-2′-eq** is only 0.8 kcal/mol, which corresponds to 4:1 dr (ax/eq) and closely mirrors the experimental outcome (5:1 dr ax/eq). DIA calculations suggest that low diastereoselectivity results from inversion of substrate−ligand NCIs compared to **L20** ($\Delta\Delta E_{\text{int-space}}$ are −4.5 and 1.6 kcal/mol for **L20** and **L21**, respectively, Figure 6B). EDA calculations show this inversion mainly arises from favorable electrostatic and dispersion interactions in **TS-2′-eq** compared to **TS-2′-ax** ($\Delta\Delta E_{\text{elstat}}$ of 1.6 kcal/mol, $\Delta\Delta E_{\text{disp}}$ of 0.4 kcal/mol) (Figure 6C). Visualization of the NCI regions (highlighted by red dots, Figure 6A) identifies a stabilizing electrostatic contribution between the carbonyl group of the substrate and the methyl group of ligand **L21** in **TS-2′-eq**. Additionally, weaker dispersion in **TS-2′-ax** owing to the smaller size of a methyl group compared to a CF_3 group contributes to comparable dispersion difference in **TS-2′-ax** and **TS-2′-eq** (Figure 6C). Taken together, these calculations reveal that substrate−ligand NCIs are the main factors that control the selectivity for the carboboration under axial-selective conditions.

Next, DFT calculations were performed to investigate the mechanism for carboborylation under equatorial-selective reaction conditions using Phosferrox ligand **L11** (see Supporting Information, Figure S10, for details). Similarly, migratory insertion was found to be the diastereoselectivity-determining step. Under these conditions, equatorial borylation is calculated to be 1.4 kcal/mol more favorable, which corresponds to a 12:1 dr (eq/ax) consistent with the experimental selectivity of 20:1 dr (eq/ax). Here again, NCI analysis, DIA, and EDA calculations were performed to investigate the origin of selectivity (see Supporting Information, Figure S11, for details). Substrate distortion and substrate−ligand steric repulsion were found to be the most significant contributors to equatorial selectivity.

CONCLUSION

Limited access to structural analogs and high synthetic costs are common barriers to the preparation and use of complex terpenoids. To ameliorate these challenges, we have developed an efficient, stereodivergent carboborylation strategy yielding diastereomeric building blocks found in thousands of natural products containing oxidized *trans*-decalin cores. Identification of axial- and equatorial-selective catalysts was accomplished through synergistic application of HTE and unsupervised diversity analysis of an in silico phosphoramidite library. Computational analysis suggests that diastereoselectivity is governed by key substrate−ligand noncovalent interactions or ligand/substrate distortion under axial- and equatorial-selective

https://doi.org/10.1021/jacs.6c01881
J. Am. Chem. Soc. XXXX, XXX, XXX−XXX

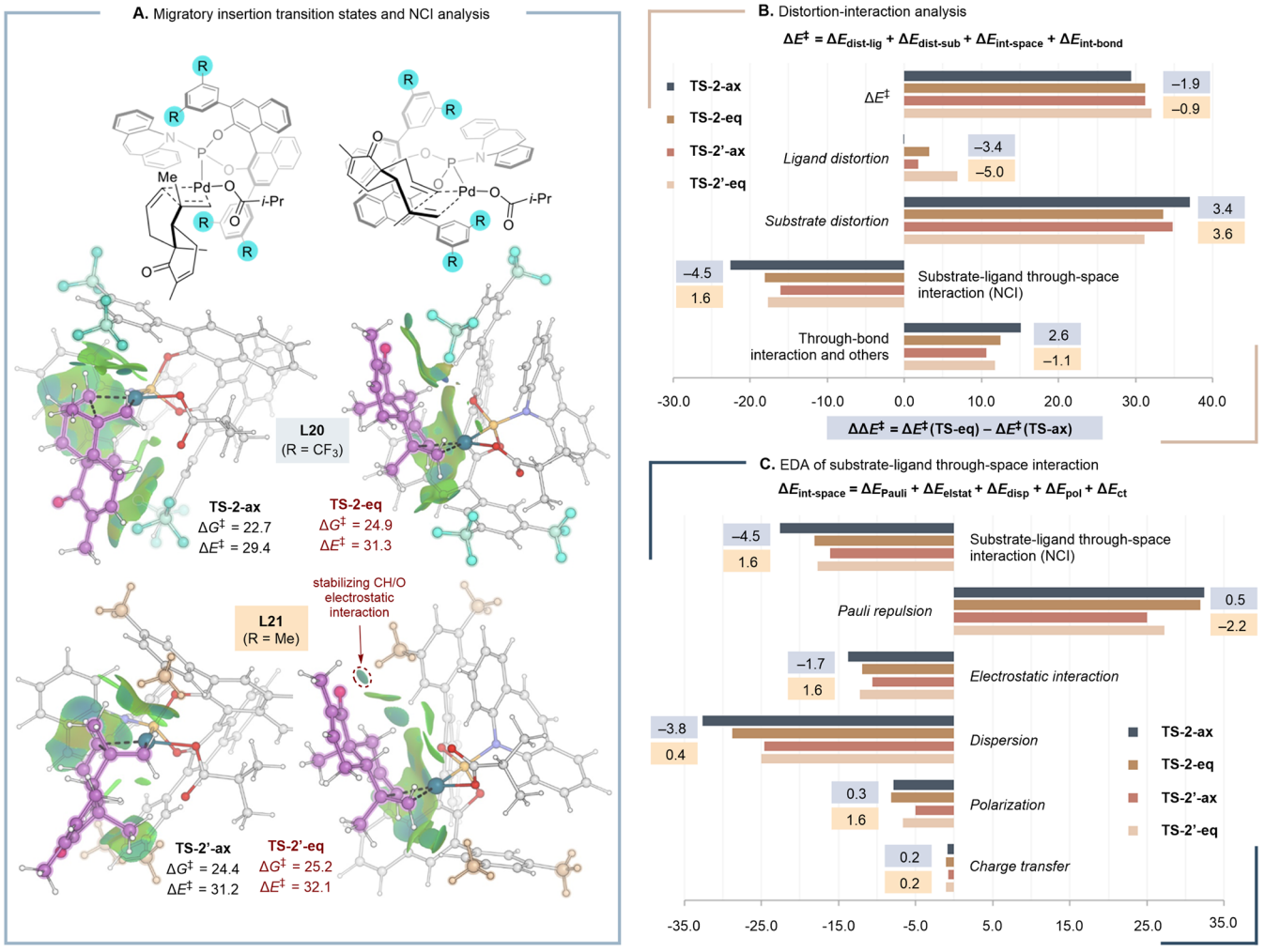

Figure 6. (A) Optimized geometries and noncovalent interaction analysis (in kcal/mol), (B) distortion-interaction analysis (DIA), and (C) energy decomposition analysis (EDA) on the migratory insertion transition states for the Pd-catalyzed carboborylation under axial-selective conditions (in kcal/mol). For B and C, numbers in boxes are energy difference between **TS-2-ax** and **TS-2-eq** (or **TS-2′-ax** and **TS-2′-eq**), in which negative and positive energy values indicate the factors that favor transition states leading to axial and equatorial products, respectively.

conditions, respectively. This method provides an advanced entry point to the synthesis of highly oxygenated terpenoid natural products, and its synthetic utility was validated in the total synthesis of several diterpenoids. We anticipate this strategy will enable the synthesis of complex bioactive terpenoids with diverse architectures.

■ ASSOCIATED CONTENT

Data Availability Statement

The data underlying this study are available in the published article and its Supporting Information.

Supporting Information

The Supporting Information is available free of charge at https://pubs.acs.org/doi/10.1021/jacs.6c01881.

Computational workflow for the construction of the phosphoramidite in silico library and selection/evaluation of the training set (PDF)

Experimental section including characterization data; NMR spectra of new compounds; supporting crystallographic information (PDF)

Accession Codes

Deposition Numbers 2473380−2473381 contain the supplementary crystallographic data for this paper. These data can be obtained free of charge via the joint Cambridge Crystallographic Data Centre (CCDC) and Fachinformationszentrum Karlsruhe Access Structures service.

■ AUTHOR INFORMATION

Corresponding Authors

David A. Petrone − *Department of Process Research & Development, MRL, Merck & Co., Inc., Rahway, New Jersey 07065, United States;* orcid.org/0000-0001-9867-9178; Email: david.petrone@merck.com

Scott E. Denmark − *Department of Chemistry, University of Illinois Urbana−Champaign, Urbana, Illinois 61801, United States;* orcid.org/0000-0002-1099-9765; Email: sdenmark@illinois.edu

David Sarlah − *Department of Chemistry, Rice University, Houston, Texas 77005, United States; Department of Chemistry, University of Illinois Urbana−Champaign, Urbana, Illinois 61801, United States;* orcid.org/0000-0002-8736-8953; Email: sarlah@rice.edu

https://doi.org/10.1021/jacs.6c01881
J. Am. Chem. Soc. XXXX, XXX, XXX−XXX

Authors

Samantha L. Barlock − *Department of Chemistry, Rice University, Houston, Texas 77005, United States; Department of Chemistry, University of Illinois Urbana−Champaign, Urbana, Illinois 61801, United States;* orcid.org/0009-0000-7215-8841

Alexander S. Shved − *Department of Chemistry, University of Illinois Urbana−Champaign, Urbana, Illinois 61801, United States;* orcid.org/0000-0001-5979-179X

Kayla D. Landers − *Department of Chemistry, Rice University, Houston, Texas 77005, United States; Department of Chemistry, University of Illinois Urbana−Champaign, Urbana, Illinois 61801, United States*

Binh Khanh Mai − *Department of Chemistry, University of Illinois Urbana−Champaign, Urbana, Illinois 61801, United States;* orcid.org/0000-0001-8487-1417

Shogo Fujiki − *Department of Chemistry, Rice University, Houston, Texas 77005, United States; Department of Chemistry, University of Illinois Urbana−Champaign, Urbana, Illinois 61801, United States;* orcid.org/0009-0009-2997-8567

Peter C. Ryffel − *Department of Chemistry, University of Illinois Urbana−Champaign, Urbana, Illinois 61801, United States*

Wai Yam Lo − *Department of Chemistry, University of Illinois Urbana−Champaign, Urbana, Illinois 61801, United States*

Andrew G. Feng − *Department of Chemistry, University of Illinois Urbana−Champaign, Urbana, Illinois 61801, United States*

Nicholas W. Wade − *Department of Chemistry, University of Illinois Urbana−Champaign, Urbana, Illinois 61801, United States*

Lingyang Zhu − *Department of Chemistry, University of Illinois Urbana−Champaign, Urbana, Illinois 61801, United States;* orcid.org/0000-0002-6657-271X

Viet D. Nguyen − *Department of Process Research & Development, MRL, Merck & Co., Inc., Rahway, New Jersey 07065, United States*

Complete contact information is available at: https://pubs.acs.org/10.1021/jacs.6c01881

Notes

The authors declare no competing financial interest.

■ ACKNOWLEDGMENTS

We acknowledge funding from the National Institutes of Health (grant GM144489 to D.S.), the Cancer Prevention and Research Institute of Texas (CPRIT, grant RR240019 to D.S.), the National Science Foundation (grant CHE 2154237 to S.E.D.), and the Naito Foundation (fellowship to S.F.). We thank Dr. Dean Olson (SCS NMR Lab, University of Illinois Urbana−Champaign) and Dr. Xu Wang (Rice University NMR Facilities) for technical support and NMR spectroscopic assistance, Eric Pettipiece and Yianni Lysandrou for assistance with X-ray crystallographic analysis, and F. Sun for assistance with mass spectrometric analysis. We also thank Kevin Belyk, Marion Emmert, and Eric Phillips for assistance with HTE studies, and Vladimir Shchurik for assistance with SFC purification (all Merck & Co., Inc., Rahway, NJ, USA). We acknowledge Sabnam Begum, Sayan Ray, Eric Pettipiece, and Emma Simmons for critical proofreading of this paper.

■ REFERENCES

(1) Gershenzon, J.; Dudareva, N. The Function of Terpene Natural Products in the Natural World. *Nat. Chem. Biol.* **2007**, *3* (7), 408−414.

(2) Zeng, T.; Liu, Z.; Zhuang, J.; Jiang, Y.; He, W.; Diao, H.; Lv, N.; Jian, Y.; Liang, D.; Qiu, Y.; Zhang, R.; Zhang, F.; Tang, X.; Wu, R. TeroKit: A Database-Driven Web Server for Terpenome Research. *J. Chem. Inf. Model.* **2020**, *60* (4), 2082−2090.

(3) Pichersky, E.; Raguso, R. A. Why Do Plants Produce so Many Terpenoid Compounds? *New Phytol.* **2018**, *220* (3), 692−702.

(4) Wang, G.; Tang, W.; Bidigare, R. R. Terpenoids As Therapeutic Drugs and Pharmaceutical Agents. In *Natural Products*, Zhang, L.; Demain, A. L., eds.; Humana Press: Totowa, NJ, 2005; pp. 197−227.

(5) Zeng, T.; Liu, Z.; Liu, H.; He, W.; Tang, X.; Xie, L.; Wu, R. Exploring Chemical and Biological Space of Terpenoids. *J. Chem. Inf. Model.* **2019**, *59* (9), 3667−3678.

(6) Jansen, D. J.; Shenvi, R. A. Synthesis of Medicinally Relevant Terpenes: Reducing the Cost and Time of Drug Discovery. *Future Med. Chem.* **2014**, *6* (10), 1127−1146.

(7) Thomas, W. P.; Pronin, S. V. New Methods and Strategies in the Synthesis of Terpenoid Natural Products. *Acc. Chem. Res.* **2021**, *54* (6), 1347−1359.

(8) Brill, Z. G.; Condakes, M. L.; Ting, C. P.; Maimone, T. J. Navigating the Chiral Pool in the Total Synthesis of Complex Terpene Natural Products. *Chem. Rev.* **2017**, *117* (18), 11753−11795.

(9) De Camp, W. H. The FDA Perspective on the Development of Stereoisomers. *Chirality* **1989**, *1* (1), 2−6.

(10) Huh, W. B.; Kim, J.-E.; Kang, Y.-G.; Park, G.; Lim, T.; Kwon, J. Y.; Song, D. S.; Jeong, E. H.; Lee, C. C.; Son, J. E.; Seo, S. G.; Lee, E.; Kim, J. R.; Lee, C. Y.; Park, J. S.; Lee, K. W. Brown Pine Leaf Extract and Its Active Component Trans-Communic Acid Inhibit UVB-Induced MMP-1 Expression by Targeting PI3K. *PLoS One* **2015**, *10* (6), No. e0128365.

(11) Shimizu, M.; Tsuji, H.; Shogawa, H.; Fukumura, H.; Tanaami, S.; Hayashi, T.; Arisawa, M.; Morita, N. Anti-Inflammatory Constituents of Topically Applied Crude Drugs. II. Constituents and Anti-Inflammatory Effect of Cryptomeria Japonica D. DON. *Chem. Pharm. Bull.* **1988**, *36* (10), 3967−3973.

(12) Hanson, J. R. Diterpenoids. *Nat. Prod. Rep.* **2009**, *26* (9), 1156.

(13) Pan, X.; Rudolf, J. D.; Dong, L.-B. Class II Terpene Cyclases: Structures, Mechanisms, and Engineering. *Nat. Prod. Rep.* **2024**, *41* (3), 402−433.

(14) Shrestha, K.; Banskota, A.H.; Kodata, S.; Shrivastava, S.P.; Strobel, G.; Gewali, M.B. An Antiproliferative Norditerpene Dilactone, Nagilactone C, From Podocarpus neriifolius. *Phytomedicine* **2001**, *8* (6), 489−491.

(15) Wafo, P.; Kamdem, R. S. T.; Ali, Z.; Anjum, S.; Khan, S. N.; Begum, A.; Krohn, K.; Abegaz, B. M.; Ngadjui, B. T.; Choudhary, M. I. Duboscic Acid: A Potent α-Glucosidase Inhibitor with an Unprecedented Triterpenoidal Carbon Skeleton from *Duboscia Macrocarpa*. *Org. Lett.* **2010**, *12* (24), 5760−5763.

(16) Fang, X. F.; Cui, Z. J. The Anti-Botulism Triterpenoid Toosendanin Elicits Calcium Increase and Exocytosis in Rat Sensory Neurons. *Cell. Mol. Neurobiol.* **2011**, *31* (8), 1151−1162.

(17) Mohamed, I. E.; Gross, H.; Pontius, A.; Kehraus, S.; Krick, A.; Kelter, G.; Maier, A.; Fiebig, H.-H.; König, G. M. Epoxyphomalin A and B, Prenylated Polyketides with Potent Cytotoxicity from the Marine-Derived Fungus *Phoma* Sp. *Org. Lett.* **2009**, *11* (21), 5014−5017.

(18) *CHEMnetBASE*. https://dnp.chemnetbase.com/chemical/ChemicalSearch.xhtml?dswid=4028. (accessed 26 February 2025).

(19) Hagiwara, H. Aspects in the Total Syntheses of Higher Terpenoids Starting From Wieland−Miescher Ketone and Its Derivative: A Review. *Nat. Prod. Commun.* **2020**, *15* (5), 1934578−20925340.

(20) Bradshaw, B.; Bonjoch, J. The Wieland-Miescher Ketone: A Journey from Organocatalysis to Natural Product Synthesis. *Synlett* **2012**, *23* (3), No. e7−e7.

(21) Hanessian, S.; Boyer, N.; Reddy, G. J.; Deschênes-Simard, B. Total Synthesis of Oidiodendrolides and Related Norditerpene Dilactones from a Common Precursor: Metabolites CJ-14,445, LL-Z1271γ, Oidiolactones A, B, C, and D, and Nagilactone F. *Org. Lett.* **2009**, *11* (20), 4640−4643.
(22) Smith, A. B.; Cho, Y. S.; Ishiyama, H. Nodulisporic Acid A Synthetic Studies. 2. Construction of an Eastern Hemisphere Subtarget. *Org. Lett.* **2001**, *3* (24), 3971−3974.
(23) Smith, A. B.; Kürti, L.; Davulcu, A. H.; Cho, Y. S. Development of a Scalable Synthesis of a Common Eastern Tricyclic Lactone for Construction of the Nodulisporic Acids. *Org. Process Res. Dev.* **2007**, *11* (1), 19−24.
(24) Trost, B. M.; Nishimura, Y.; Yamamoto, K. A Total Synthesis of Aphidicolin. *J. Am. Chem. Soc.* **1979**, *101* (5), 1328−1330.
(25) Reuvers, J. T. A.; De Groot, A. Stereoselective Synthesis of (.±.)-3,4,4a,5,6,7,8,8a-Octahydronaphthalen-1(2H)-Ones via Homogeneous Hydrogenation of (.±.)-5,6,7,8-Tetrahydronaphthalenones. *J. Org. Chem.* **1984**, *49* (6), 1110−1113.
(26) Bogenstätter, M.; Limberg, A.; Overman, L. E.; Tomasi, A. L. Enantioselective Total Synthesis of the Kinesin Motor Protein Inhibitor Adociasulfate 1. *J. Am. Chem. Soc.* **1999**, *121* (51), 12206−12207.
(27) Snider, B. B.; Mohan, R.; Kates, S. A. Manganese(III)-Based Oxidative Free-Radical Cyclization. Synthesis of (.±.)-Podocarpic Acid. *J. Org. Chem.* **1985**, *50* (19), 3659−3661.
(28) Barrero, A. F.; Quílez Del Moral, J. F.; Herrador, M. M.; Loayza, I.; Sánchez, E. M.; Arteaga, J. F. Synthesis of Five- to Seven-Membered Polyfunctional Terpenic Carbocycles via Ti(III)-Catalyzed Radical Cyclizations of Epoxypolyprenes. *Tetrahedron* **2006**, *62* (22), 5215−5222.
(29) Odani, A.; Ishihara, K.; Ohtawa, M.; Tomoda, H.; Omura, S.; Nagamitsu, T. Total Synthesis of Pyripyropene A. *Tetrahedron* **2011**, *67* (42), 8195−8203.
(30) Li, T.; Wu, G.; Feng, S.; Wang, Z.; Xie, X.; She, X. A Rapid Construction of the ABC Tricyclic Skeleton of Malabanone A. *Org. Biomol. Chem.* **2018**, *16* (44), 8491−8494.
(31) Hua, D. H.; Takasu, K.; Huang, X.; Millward, G. S.; Chen, Y.; Fan, J. Palladium-Mediated Ring Closure Reactions. Facile Syntheses of Enantiopure Bicyclic and Tricyclic Alkenones. *Tetrahedron* **2000**, *56* (38), 7389−7398.
(32) Baldwin, J. E.; Jones, R. H.; Najera, C.; Yus, M. Functionalisation of Unactivated Methyl Groups through Cyclopalladation Reactions. *Tetrahedron* **1985**, *41* (4), 699−711.
(33) Bore, L.; Honda, T.; Gribble, G. W. Synthesis of β-Boswellic Acid Analogues with a Carboxyl Group at C-17 Isolated from the Bark of *Schefflera o Ctophylla*. *J. Org. Chem.* **2000**, *65* (19), 6278−6282.
(34) Simmons, E. M.; Hartwig, J. F. Catalytic Functionalization of Unactivated Primary C−H Bonds Directed by an Alcohol. *Nature* **2012**, *483* (7387), 70−73.
(35) Deng, H.; Deng, H.; Kim, C.; Li, P.; Wang, X.; Yu, Y.; Qin, T. Synthesis of Nimbolide and Its Analogues and Their Application as Poly(ADP-Ribose) Polymerase-1 Trapping Inducers. *Nat. Synth.* **2024**, *3* (3), 378−385.
(36) Grigg, R.; Sansano, J.; Santhakumar, V.; Sridharan, V.; Thangavelanthum, R.; Thornton-Pett, M.; Wilson, D. Palladium Catalysed Tandem Cyclisation-Anion Capture Processes. Part 3. Organoboron Anion Transfer Agents. *Tetrahedron* **1997**, *53* (34), 11803−11826.
(37) Grigg, R.; Sridharan, V. Palladium Catalysed Cascade Cyclisation-Anion Capture, Relay Switches and Molecular Queues. *J. Organomet. Chem.* **1999**, *576* (1−2), 65−87.
(38) Pinto, A.; Jia, Y.; Neuville, L.; Zhu, J. Palladium-Catalyzed Enantioselective Domino Heck−Cyanation Sequence: Development and Application to the Total Synthesis of Esermethole and Physostigmine. *Chem. − Eur. J.* **2007**, *13* (3), 961−967.
(39) Hong, Y.; Liu, W.; Dong, M.; Chen, X.; Xu, T.; Tian, P.; Tong, X. Pd(0)-Catalyzed Cyclizative Phosphorylation of (Z)-1-Iodo-1,6-Diene: Synthesis of Alkylphosphonate and Alkylthionophosphonate. *Org. Lett.* **2019**, *21* (14), 5742−5746.
(40) Hosoya, Y.; Kobayashi, I.; Mizoguchi, K.; Nakada, M. Palladium-Catalyzed Carbothiolation via Trapping of the σ-Alkyl Palladium Intermediate with RSTIPS. *Org. Lett.* **2019**, *21* (20), 8280−8284.
(41) Ping, Y.; Li, Y.; Zhu, J.; Kong, W. Construction of Quaternary Stereocenters by Palladium-Catalyzed Carbopalladation-Initiated Cascade Reactions. *Angew. Chem. Int. Ed.* **2019**, *58* (6), 1562−1573.
(42) Wu, X.-X.; Ye, H.; Jiang, G.; Hu, L. Domino Heck/Hiyama Cross-Coupling: Trapping of the σ-Alkylpalladium Intermediate with Arylsilanes. *Org. Biomol. Chem.* **2021**, *19* (19), 4254−4257.
(43) Yoon, H.; Petrone, D. A.; Lautens, M. Diastereoselective Palladium-Catalyzed Arylcyanation/Heteroarylcyanation of Enantioenriched *N* -Allylcarboxamides. *Org. Lett.* **2014**, *16* (24), 6420−6423.
(44) Vachhani, D. D.; Butani, H. H.; Sharma, N.; Bhoya, U. C.; Shah, A. K.; Van Der Eycken, E. V. Domino Heck/Borylation Sequence towards Indolinone-3-Methyl Boronic Esters: Trapping of the σ-Alkylpalladium Intermediate with Boron. *Chem. Commun.* **2015**, *51* (80), 14862−14865.
(45) Jiang, Z.; Hou, L.; Ni, C.; Chen, J.; Wang, D.; Tong, X. Enantioselective Construction of Quaternary Tetrahydropyridines by Palladium-Catalyzed Vinylborylation of Alkenes. *Chem. Commun.* **2017**, *53* (30), 4270−4273.
(46) Lu, H.; Yang, X.; Zhou, L.; Li, W.; Deng, G.; Yang, Y.; Liang, Y. Palladium-Catalyzed Domino Heck-Disilylation and -Borylation of Alkene-Tethered 2-(2-Halophenyl)-1 *H* -Indoles: Access to Diverse Disilylated and Borylated Indolo[2,1- *a*]Isoquinolines. *Org. Chem. Front.* **2020**, *7* (15), 2016−2021.
(47) Bai, X.; Zheng, W.; Ge, S.; Lu, Y. Enantioselective Palladium-Catalyzed Arylborylation/Cyclization of Alkenes to Access Boryl-Functionalized Heterocyclic Compounds Containing Quaternary Stereogenic Centers. *Org. Lett.* **2022**, *24* (16), 3080−3085.
(48) Yoon, H.; Jang, Y.; Lautens, M. Diastereoselective Pd-Catalyzed Domino Heck/Arylborylation Sequence Forming Borylated Chromans. *Synthesis* **2016**, *48* (10), 1483−1490.
(49) Ryffel, D. B.; Ryffel, P. C.; Martinelli, M.; Pillai, V. R.; Sarlah, D. Stereoselective Total Synthesis of Nimbolide. *J. Am. Chem. Soc.* **2025**, *147* (17), 14083−14087.
(50) Ashimori, A.; Bachand, B.; Calter, M. A.; Govek, S. P.; Overman, L. E.; Poon, D. J. Catalytic Asymmetric Synthesis of Quaternary Carbon Centers. Exploratory Studies of Intramolecular Heck Reactions of (*Z*)-α,β-Unsaturated Anilides and Mechanistic Investigations of Asymmetric Heck Reactions Proceeding via Neutral Intermediates. *J. Am. Chem. Soc.* **1998**, *120* (26), 6488−6499.
(51) Ito, T.; Takahashi, Y.; Ishii, Y. Convenient Preparation of Novel Palladium−π-Olefin Complexes from Bis(Dibenzylideneacetone)-Palladium(0). *J. Chem. Soc., Chem. Commun.* **1972**, No. 11, 629a−629a.
(52) Zalesskiy, S. S.; Ananikov, V. P. $Pd_2(Dba)_3$ as a Precursor of Soluble Metal Complexes and Nanoparticles: Determination of Palladium Active Species for Catalysis and Synthesis. *Organometallics* **2012**, *31* (6), 2302−2309.
(53) Ueda, S.; Su, M.; Buchwald, S. L. Completely N^1 -Selective Palladium-Catalyzed Arylation of Unsymmetric Imidazoles: Application to the Synthesis of Nilotinib. *J. Am. Chem. Soc.* **2012**, *134* (1), 700−706.
(54) Huang, J.; Isaac, M.; Watt, R.; Becica, J.; Dennis, E.; Saidaminov, M. I.; Sabbers, W. A.; Leitch, D. C. ^{DMP} DAB−Pd−MAH: A Versatile Pd(0) Source for Precatalyst Formation, Reaction Screening, and Preparative-Scale Synthesis. *ACS Catal.* **2021**, *11* (9), 5636−5646.
(55) Krska, S. W.; DiRocco, D. A.; Dreher, S. D.; Shevlin, M. The Evolution of Chemical High-Throughput Experimentation To Address Challenging Problems in Pharmaceutical Synthesis. *Acc. Chem. Res.* **2017**, *50* (12), 2976−2985.
(56) Mennen, S. M.; Alhambra, C.; Allen, C. L.; Barberis, M.; Berritt, S.; Brandt, T. A.; Campbell, A. D.; Castañón, J.; Cherney, A.

https://doi.org/10.1021/jacs.6c01881
J. Am. Chem. Soc. XXXX, XXX, XXX−XXX

H.; Christensen, M.; Damon, D. B.; Eugenio De Diego, J.; García-Cerrada, S.; García-Losada, P.; Haro, R.; Janey, J.; Leitch, D. C.; Li, L.; Liu, F.; Lobben, P. C.; MacMillan, D. W. C.; Magano, J.; McInturff, E.; Monfette, S.; Post, R. J.; Schultz, D.; Sitter, B. J.; Stevens, J. M.; Strambeanu, I. I.; Twilton, J.; Wang, K.; Zajac, M. A. The Evolution of High-Throughput Experimentation in Pharmaceutical Development and Perspectives on the Future. *Org. Process Res. Dev.* **2019**, *23* (6), 1213−1242.
(57) Gensch, T.; Dos Passos Gomes, G.; Friederich, P.; Peters, E.; Gaudin, T.; Pollice, R.; Jorner, K.; Nigam, A.; Lindner-D'Addario, M.; Sigman, M. S.; Aspuru-Guzik, A. A Comprehensive Discovery Platform for Organophosphorus Ligands for Catalysis. *J. Am. Chem. Soc.* **2022**, *144* (3), 1205−1217.
(58) Gensch, T.; Smith, S. R.; Colacot, T. J.; Timsina, Y. N.; Xu, G.; Glasspoole, B. W.; Sigman, M. S. Design and Application of a Screening Set for Monophosphine Ligands in Cross-Coupling. *ACS Catal.* **2022**, *12* (13), 7773−7780.
(59) Santiago, C. B.; Guo, J.-Y.; Sigman, M. S. Predictive and Mechanistic Multivariate Linear Regression Models for Reaction Development. *Chem. Sci.* **2018**, *9* (9), 2398−2412.
(60) Zahrt, A. F.; Athavale, S. V.; Denmark, S. E. Quantitative Structure−Selectivity Relationships in Enantioselective Catalysis: Past, Present, and Future. *Chem. Rev.* **2020**, *120* (3), 1620−1689.
(61) Zahrt, A. F.; Henle, J. J.; Rose, B. T.; Wang, Y.; Darrow, W. T.; Denmark, S. E. Prediction of Higher-Selectivity Catalysts by Computer-Driven Workflow and Machine Learning. *Science* **2019**, *363* (6424), No. eaau5631.
(62) Henle, J. J.; Zahrt, A. F.; Rose, B. T.; Darrow, W. T.; Wang, Y.; Denmark, S. E. Development of a Computer-Guided Workflow for Catalyst Optimization. Descriptor Validation, Subset Selection, and Training Set Analysis. *J. Am. Chem. Soc.* **2020**, *142* (26), 11578−11592.
(63) Rose, B. T.; Timmerman, J. C.; Bawel, S. A.; Chin, S.; Zhang, H.; Denmark, S. E. High-Level Data Fusion Enables the Chemoinformatically Guided Discovery of Chiral Disulfonimide Catalysts for Atropselective Iodination of 2-Amino-6-Arylpyridines. *J. Am. Chem. Soc.* **2022**, *144* (50), 22950−22964.
(64) Olen, C. L.; Zahrt, A. F.; Reilly, S. W.; Schultz, D.; Emerson, K.; Candito, D.; Wang, X.; Strotman, N. A.; Denmark, S. E. Chemoinformatic Catalyst Selection Methods for the Optimization of Copper−Bis(Oxazoline)-Mediated, Asymmetric, Vinylogous Mukaiyama Aldol Reactions. *ACS Catal.* **2024**, *14* (4), 2642−2655.
(65) Shved, A. S.; Ocampo, B. E.; Burlova, E. S.; Olen, C. L.; Rinehart, N. I.; Denmark, S. E. Molli: A General Purpose Python Toolkit for Combinatorial Small Molecule Library Generation, Manipulation, and Feature Extraction. *J. Chem. Inf. Model.* **2024**, *64* (21), 8083−8090.
(66) Zahrt, A. F.; Rose, B. T.; Darrow, W. T.; Henle, J. J.; Denmark, S. E. Computational Methods for Training Set Selection and Error Assessment Applied to Catalyst Design: Guidelines for Deciding Which Reactions to Run First and Which to Run Next. *React. Chem. Eng.* **2021**, *6* (4), 694−708.
(67) Grimme, S. Exploration of Chemical Compound, Conformer, and Reaction Space with Meta-Dynamics Simulations Based on Tight-Binding Quantum Chemical Calculations. *J. Chem. Theory Comput.* **2019**, *15* (5), 2847−2862.
(68) Bannwarth, C.; Ehlert, S.; Grimme, S. GFN2-xTB−An Accurate and Broadly Parametrized Self-Consistent Tight-Binding Quantum Chemical Method with Multipole Electrostatics and Density-Dependent Dispersion Contributions. *J. Chem. Theory Comput.* **2019**, *15* (3), 1652−1671.
(69) Landrum, G.; Tosco, P.; Kelley, B.; Rodriguez, R.; Cosgrove, D.; Vianello, R.; Sriniker, P. G.; Jones, G.; Kawashima, E.; NadineSchneider, D. N.; et al.. *Rdkit/Rdkit: 2025_09_4 (Q3 2025) Release*; ZENODO, 2025.
(70) *RDKit*. https://rdkit.org/. (accessed 25 January 2026).
(71) Barroso, S.; Joksch, M.; Puylaert, P.; Tin, S.; Bell, S. J.; Donnellan, L.; Duguid, S.; Muir, C.; Zhao, P.; Farina, V.; Tran, D. N.; De Vries, J. G. Improvement in the Palladium-Catalyzed Miyaura Borylation Reaction by Optimization of the Base: Scope and Mechanistic Study. *J. Org. Chem.* **2021**, *86* (1), 103−109.
(72) González, M. A. Aromatic Abietane Diterpenoids: Their Biological Activity and Synthesis. *Nat. Prod. Rep.* **2015**, *32* (5), 684−704.
(73) Da Silva Rodrigues-Corrêa, K. C.; De Lima, J. C.; Fett-Neto, A. G. Oleoresins from Pine: Production and Industrial Uses. In *Natural Products*, Ramawat, K. G.; Mérillon, J.-M., eds; Springer Berlin Heidelberg: Berlin, Heidelberg, 2013; pp. 4037−4060.
(74) Wang, Y.-D.; Zhang, G.-J.; Qu, J.; Li, Y.-H.; Jiang, J.-D.; Liu, Y.-B.; Ma, S.-G.; Li, Y.; Lv, H.-N.; Yu, S.-S. Diterpenoids and Sesquiterpenoids from the Roots of *Illicium Majus*. *J. Nat. Prod.* **2013**, *76* (10), 1976−1983.
(75) González, M. A.; Zaragozá, R. J. Semisynthesis of the Antiviral Abietane Diterpenoid Jiadifenoic Acid C from Callitrisic Acid (4-Epidehydroabietic Acid) Isolated from Sandarac Resin. *J. Nat. Prod.* **2014**, *77* (9), 2114−2117.
(76) Pelletier, S. W.; Herald, D. L. Inversion of the C-4 Substituents in Dehydroabietic Acid: Synthesis of (+)-Callitrisic Acid. *J. Chem. Soc., Chem. Commun.* **1971**, No. 1, 10b.
(77) Alvarez-Manzaneda, E.; Chahboun, R.; Alvarez, E.; Ramos, J.; Guardia, J.; Messouri, I.; Chayboun, I.; Mansour, A.; Dahdouh, A. Synthesis of (+)-Hanagokenol A, (+)-Fortunins E, G, H, and (−)-Sugikurojin A from Abietic Acid. *Synthesis* **2010**, *2010* (20), 3493−3503.
(78) Finkbeiner, P.; Murai, K.; Röpke, M.; Sarpong, R. Total Synthesis of Terpenoids Employing a "Benzannulation of Carvone" Strategy: Synthesis of (−)-Crotogoudin. *J. Am. Chem. Soc.* **2017**, *139* (33), 11349−11352.
(79) Zhang, K.; Christoffel, F.; Baudoin, O. Barbier−Negishi Coupling of Secondary Alkyl Bromides with Aryl and Alkenyl Triflates and Nonaflates. *Angew. Chem. Int. Ed.* **2018**, *57* (7), 1982−1986.
(80) Ulubelen, A.; Topcu, G. Abietane Diterpenoids from Salvia Pomifera. *Phytochemistry* **1992**, *31* (11), 3949−3951.
(81) Yang, X.-W.; Feng, L.; Li, S.-M.; Liu, X.-H.; Li, Y.-L.; Wu, L.; Shen, Y.-H.; Tian, J.-M.; Zhang, X.; Liu, X.-R.; Wang, N.; Liu, Y.; Zhang, W.-D. Isolation, Structure, and Bioactivities of Abiesadines A−Y, 25 New Diterpenes from Abies Georgei Orr. *Bioorg. Med. Chem.* **2010**, *18* (2), 744−754.
(82) Tanaka, R.; Ohtsu, H.; Matsunaga, S. Abietane Diterpene Acids and Other Constituents from the Leaves of Larix Kaempferi. *Phytochemistry* **1997**, *46* (6), 1051−1057.
(83) Yuan, C.; Eliasen, A. M.; Camelio, A. M.; Siegel, D. Preparation of Phenols by Phthaloyl Peroxide−Mediated Oxidation of Arenes. *Nat. Protoc.* **2014**, *9* (11), 2624−2629.
(84) Harrison, L. J.; Asakawa, Y. 18-Oxoferruginol from the Leaf of Torreya Nucifera. *Phytochemistry* **1987**, *26* (4), 1211−1212.
(85) Chamy, M. C.; Piovano, M.; Garbarino, J. A.; Chaparro, A. Diterpenoids from Calceolaria Hypericina. *Phytochemistry* **1995**, *40* (4), 1209−1212.
(86) Wu, X.-D.; Luo, D.; Tu, W.-C.; Deng, Z.-T.; Chen, X.-J.; Su, J.; Ji, X.; Zhao, Q.-S. Hypophyllins A−D, Labdane-Type Diterpenoids with Vasorelaxant Activity from *Hypoestes Phyllostachya* "Rosea". *Org. Lett.* **2016**, *18* (24), 6484−6487.
(87) Osborn, J. A.; Jardine, F. H.; Young, J. F.; Wilkinson, G. The Preparation and Properties of Tris(Triphenylphosphine)-Halogenorhodium(I) and Some Reactions Thereof Including Catalytic Homogeneous Hydrogenation of Olefins and Acetylenes and Their Derivatives. *J. Chem. Soc. A* **1966**, 1711−1732.
(88) Shibuya, M.; Tomizawa, M.; Suzuki, I.; Iwabuchi, Y. 2-Azaadamantane *N* -Oxyl (AZADO) and 1-Me-AZADO: Highly Efficient Organocatalysts for Oxidation of Alcohols. *J. Am. Chem. Soc.* **2006**, *128* (26), 8412−8413.
(89) Kuwajima, I.; Urabe, H. Regioselective Arylation of Silyl Enol Ethers of Methyl Ketones with Aryl Bromides. *J. Am. Chem. Soc.* **1982**, *104* (24), 6831−6833.
(90) Benítez, A.; Herrera, F. R.; Romero, M.; Talamás, F. X.; Muchowski, J. M. Site Selectivity of the Diels−Alder Reactions of 3-

https://doi.org/10.1021/jacs.6c01881
J. Am. Chem. Soc. XXXX, XXX, XXX−XXX

[1-(*Tert* -Butyldimethylsilyloxy)Vin-1-Yl]Furan and 3-(Propen-2-Yl)-Furan. Synthesis of 4-Substituted Benzofurans. *J. Org. Chem.* **1996**, *61* (4), 1487−1492.
(91) Wüstenberg, B.; Pfaltz, A. Homogeneous Hydrogenation of Tri- and Tetrasubstituted Olefins: Comparison of Iridium-Phosphinooxazoline [Ir-PHOX] Complexes and Crabtree Catalysts with Hexafluorophosphate (PF_6) and Tetrakis[3,5-bis(Trifluoromethyl)-Phenyl]Borate (BAr_F) as Counterions. *Adv. Synth. Catal.* **2008**, *350* (1), 174−178.
(92) Frigerio, M.; Santagostino, M. A Mild Oxidizing Reagent for Alcohols and 1,2-Diols: O-Iodoxybenzoic Acid (IBX) in DMSO. *Tetrahedron Lett* **1994**, *35* (43), 8019−8022.
(93) Peccati, F. NCIPLOT4 Guide for Biomolecules: An Analysis Tool for Noncovalent Interactions. *J. Chem. Inf. Model.* **2020**, *60* (1), 6−10.
(94) Gramüller, J.; Gschwind, R. M. An NMR Spectroscopy View on London Dispersion in Catalysis: Detection, Quantification, and Application in Ion Pair and Transition Metal Catalysis. *Acc. Chem. Res.* **2023**, *56* (21), 2968−2979.
(95) Hartmann, E.; Gschwind, R. M. The Supramolecular Balance for Transition-Metal Complexes: Assessment of Noncovalent Interactions in Phosphoramidite Palladium Complexes. *Angew. Chem. Int. Ed.* **2013**, *52* (8), 2350−2354.
(96) Hartmann, E.; Hammer, M. M.; Gschwind, R. M. Structures and Interligand Interaction Pattern of Phosphoramidite Pd Complexes by NMR Spectroscopy: Modulations in Extended Interaction Surfaces as Stereoselection Mode of a Privileged Class of Ligands. *Chem. − Eur. J.* **2013**, *19* (32), 10551−10562.
(97) Ess, D. H.; Houk, K. N. Distortion/Interaction Energy Control of 1,3-Dipolar Cycloaddition Reactivity. *J. Am. Chem. Soc.* **2007**, *129* (35), 10646−10647.
(98) Bickelhaupt, F. M.; Houk, K. N. Analyzing Reaction Rates with the Distortion/Interaction-Activation Strain Model. *Angew. Chem. Int. Ed.* **2017**, *56* (34), 10070−10086.
(99) Lu, G.; Liu, R. Y.; Yang, Y.; Fang, C.; Lambrecht, D. S.; Buchwald, S. L.; Liu, P. Ligand−Substrate Dispersion Facilitates the Copper-Catalyzed Hydroamination of Unactivated Olefins. *J. Am. Chem. Soc.* **2017**, *139* (46), 16548−16555.
(100) Xi, Y.; Su, B.; Qi, X.; Pedram, S.; Liu, P.; Hartwig, J. F. Application of Trimethylgermanyl-Substituted Bisphosphine Ligands with Enhanced Dispersion Interactions to Copper-Catalyzed Hydroboration of Disubstituted Alkenes. *J. Am. Chem. Soc.* **2020**, *142* (42), 18213−18222.
(101) Hohenstein, E. G.; Sherrill, C. D. Wavefunction Methods for Noncovalent Interactions. *Wiley Interdiscip. Rev.: Comput. Mol. Sci.* **2012**, *2* (2), 304−326.
(102) Szalewicz, K. Symmetry-adapted Perturbation Theory of Intermolecular Forces. *Wiley Interdiscip. Rev.: Comput. Mol. Sci.* **2012**, *2* (2), 254−272.

https://doi.org/10.1021/jacs.6c01881
J. Am. Chem. Soc. XXXX, XXX, XXX−XXX